

2D Magneto-Optical Trapping of Diatomic Molecules

Matthew T. Hummon,^{*} Mark Yeo, Benjamin K. Stuhl,[†] Alejandra L. Collopy, Yong Xia,[‡] and Jun Ye
*JILA, National Institute of Standards and Technology and University of Colorado, Boulder, Colorado 80309-0440,
 USA and Department of Physics, University of Colorado, Boulder, Colorado 80309-0390, USA*

(Received 4 October 2012; published 1 April 2013)

We demonstrate one- and two-dimensional transverse laser cooling and magneto-optical trapping of the polar molecule yttrium (II) oxide (YO). In a 1D magneto-optical trap (MOT), we characterize the magneto-optical trapping force and decrease the transverse temperature by an order of magnitude, from 25 to 2 mK, limited by interaction time. In a 2D MOT, we enhance the intensity of the YO beam and reduce the transverse temperature in both transverse directions. The approach demonstrated here can be applied to many molecular species and can also be extended to 3D.

DOI: [10.1103/PhysRevLett.110.143001](https://doi.org/10.1103/PhysRevLett.110.143001)

PACS numbers: 37.10.Mn, 37.10.Pq, 37.10.Vz

Over the past quarter century, the magneto-optical trap (MOT) has been extended to two dozen atomic species [1]. This abundance of species makes ultracold atomic systems a powerful tool for studying diverse phenomena, from quantum-degenerate gases, physics beyond the standard model [2], and strongly correlated systems [3] to applications in quantum information [4] and simulation, quantum sensing, and ultraprecise optical clocks [5]. Ultracold polar molecules, with their additional internal degrees of freedom and complex interactions, yield even richer phenomena [6]. Trapped ultracold samples of molecules promise to enhance the sensitivity of tests of fundamental symmetries [7–9], study complex quantum systems under precise control, produce new ultracold samples of atomic species not available with current cooling techniques [10,11], and open the door to ultracold chemistry via production of ultracold organic molecules [11,12].

Recently, many techniques have been developed for producing cold and ultracold samples of polar molecules. Magnetoassociation and the adiabatic transfer [13] of ultracold atoms can produce ultracold samples of polar molecules, although this technique is currently limited to alkali species. Buffer gas cooling [14] and molecular beam slowing techniques, such as Stark [15] and Zeeman [16,17] deceleration, can produce molecules cold enough to load into conservative traps. Further cooling of these trapped samples to temperatures below 10 mK via evaporative or sympathetic cooling is possible [18] but remains technically challenging. Optoelectric cooling of CH₃F molecules has resulted in temperatures as low as 29 mK [12]. Optical cooling has been proposed [19,20] and recently realized [21]. A MOT [20] would be the ideal tool for producing ultracold trapped samples of diatomic molecules, much as it is for atoms.

A MOT gains its utility by combining a spatially dependent trapping force with a fast dissipative cooling force. With cooling rates on the order of 10^5 s⁻¹, warm atoms can be cooled and compressed in a few milliseconds over length scales of less than 1 cm, with 2D MOTs producing

high intensity beams of cold atoms [22] and 3D MOTs producing cold, dense trapped samples. The realization of a molecular MOT will dramatically lengthen the interaction and observation times for molecules as well as increase the molecular densities and collision rates. Enhanced collision rates are necessary for applications such as ultracold chemistry and evaporative cooling.

In this Letter, we demonstrate a method for producing both a dissipative cooling and a magneto-optical spring force for diatomic molecules using oscillating magnetic fields and time-dependent optical polarizations. We demonstrate and characterize the technique for the molecule yttrium (II) oxide (YO) in both 1D and 2D MOT configurations, using one main cooling laser and two additional repumping lasers. To achieve the fast cooling rates necessary for MOT, more than 10^4 optical photons must be scattered at rates of $\sim 10^6$ s⁻¹, requiring a highly closed electronic transition, despite the presence of the additional vibrational and rotational degrees of freedom. The demonstrated method is, however, quite general and can be applied to molecular species with quasicycling transitions between electronic states with unequal magnetic moments, with only a minimal increase in laser complexity [19,20]. Indeed, two dozen suitable diatomic molecular systems have been identified [7–11,19–21,23], with species including hydrides, carbides, halides, and oxides, promising a diverse set of physical and chemical phenomena. We note that a fast dissipative cooling force for SrF molecules has been observed experimentally in 1D transverse laser cooling [21] and longitudinal slowing [24] of a SrF beam.

YO has a single naturally abundant isotopomer ⁸⁹Y¹⁶O and a relatively simple hyperfine structure with nuclear spins $\mathbf{I}_Y = 1/2$ and $\mathbf{I}_O = 0$. The main cooling transition proceeds on $X^2\Sigma^+ \rightarrow A^2\Pi_{1/2}$ at 614 nm, as shown in Fig. 1(a). The $A^2\Pi_{1/2}$ has a radiative lifetime of $\gamma^{-1} = 33$ ns [25], allowing for fast optical cycling. Diagonal Franck-Condon factors limit the vibrational branching of $A^2\Pi_{1/2}$ [26]. Only two additional lasers at 648 and 649 nm

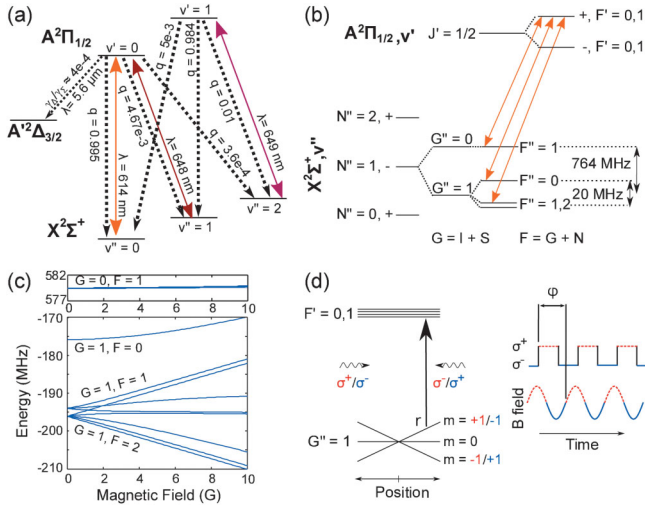


FIG. 1 (color). (a) YO vibronic structure. The dashed arrows indicate decay paths with corresponding Franck-Condon factors q [26]. The solid arrows indicate cooling and repump laser transitions. (b) Rotational and hyperfine structure of the X and A states. The solid arrows indicate the three hyperfine pumping components used in this work. (c) Zeeman structure for the $X^2\Sigma^+$, $N'' = 1$ state. (d) Schematic of the MOT level structure and the modulation waveforms for optical polarization and magnetic field.

to repump the $v'' = 1, 2$ levels are needed to limit the vibrational branching loss to $< 10^{-6}$. The loss will likely be dominated by branching to the intermediate electronic state $A^2\Delta_{3/2}$ at a level of $\eta < 4 \times 10^{-4}$ [27,28]. The $|A, v'; J' = 1/2, F', +\rangle$ manifold forms a highly closed transition with the $|X, v''; N'' = 1, G'', F'', -\rangle$ manifold, as shown in Fig. 1(b), due to parity and angular momentum selection rules [20,27,29]. The molecular states are labeled by quantum numbers for vibration v , total angular momentum excluding nuclear spin J , rotation N , intermediate quantum number G formed by coupling of electron and nuclear spin $\mathbf{G} = \mathbf{S} + \mathbf{I}$, total angular momentum F , and parity $p = \pm$ [27,30]. The repumping of hyperfine levels within each vibrational level is achieved with a single laser by creating frequency shifted sidebands using an acousto-optic modulator [27]. In order to maintain optimal photon scattering rates for laser cooling, we destabilize optical dark states that form in the ground state Zeeman manifolds [31] by modulating the polarization of the cooling light between σ^+ and σ^- with a voltage-controlled wave plate (a Pockels cell). The modulation rate should be similar to the optical pumping rate, which in our case is on the order of several 10^6 s^{-1} .

This laser configuration for creating a quasicycling transition is used for Doppler cooling of molecules [27] and for creating a MOT. The magnetic field dependence of the ground manifold is shown in Fig. 1(c) [32]; the $A^2\Pi_{1/2}$ state is magnetically insensitive. Figure 1(d) shows the simplified YO level structure involved in the MOT. In contrast to a typical atomic MOT, the ground state has a

larger Zeeman degeneracy than the excited electronic state. A quadrupole magnetic field gradient provides a spatially dependent energy shift of the $G'' = 1$ ground state. A molecule at position r [Fig. 1(d)] in the upper Zeeman level preferentially scatters photons from the laser propagating to the left due to selection rules and laser detunings. This results in a restoring force toward the center of the trap (magnetic field minimum). Since we modulate the cooling light polarization to destabilize dark states, we must also modulate the direction of the magnetic field in phase with the light polarization to maintain a restoring force for the MOT. This is shown schematically in Fig. 1(d). Atomic MOTs with magnetic fields oscillating at 5 kHz can produce stable three-dimensional trapping [33]. Our modulation frequency of 2 MHz is set by the optical pumping rate. The MOT method described here is applicable to a wide class of molecules since it requires only a differential Zeeman shift between the ground and excited electronic states. For molecules with a more complicated hyperfine structure than shown in Fig. 1(d), it is straightforward to choose the correct laser polarization for each hyperfine manifold.

To fully describe the cooling and trapping forces for YO would involve 44 molecular levels, 15 optical frequencies with time-dependent polarization, and a time-dependent magnetic field. Nevertheless, a simple multilevel rate equation (MLRE) model [34] can be used to extend the results from the two-level models to provide physical insight into the observed dynamics of a YO MOT. In the limit of small laser detunings and low laser power, the optical cooling and trapping force for the two-level system in one dimension can be expressed in the form $F_{\text{MO}} = -\beta v - \kappa r$ [27,35]. Here, F_{MO} is the force experienced by the molecule; β characterizes a viscous cooling (Doppler) force, proportional to the molecule's velocity v ; and κ represents a magneto-optical spring force proportional to the molecule's displacement r from the magnetic field minimum. κ can be expressed in terms of β as $\kappa = \mu' A \beta / \hbar k$, where μ' is the differential magnetic moment between the ground and excited states, A is the magnetic field gradient, k is the wave number, and \hbar is the reduced Planck constant.

For multilevel systems with N ground states and a single excited state, the optimal (maximum) damping parameter β_N scales roughly as $\beta_N \sim 2\beta_1 / (N + 1)$ and is achieved when all ground states are driven [27]. Despite slower damping rates, the Doppler cooling limit for the multilevel system remains unchanged from the two-level result, $T_{\text{Dop}} = \hbar \gamma / 2k_B = 116 \mu\text{K}$. The slower damping rates are balanced by slower heating rates from photon recoils. For our time-dependent magnetic field, it suffices to replace the two-level system κ with a time averaged $\bar{\kappa}$. Averaging the magneto-optical force over a single cycle yields $\bar{\kappa} = (2\sqrt{2}/\pi) \cos(\varphi) (\mu' A_{\text{rms}} \beta / \hbar k)$, where A_{rms} is the root-mean-square (rms) field gradient and φ is the

phase between the modulation of the MOT field and the optical polarization. By changing the relative phase φ , we can change the magnitude and sign of the MOT spring force independently of the Doppler force.

To characterize the MOT, we use a cryogenic buffer gas molecular beam apparatus [36], depicted in Fig. 2. The YO molecules are produced via laser ablation of a sintered Y_2O_3 pellet located inside a copper cell filled with a 4.5 K helium buffer gas. The YO molecules thermalize translationally and rotationally via collisions with the 4.5 K helium buffer gas. In-cell laser absorption measurements indicate initial $|X, 0; N'' = 1\rangle$ densities on the order of 10^{10} cm^{-3} , corresponding to more than 10^{10} molecules produced per ablation pulse. A YO molecular beam is formed by extraction of the molecules through a 3 mm diameter aperture in the side of the buffer gas cell. The molecular beam is collimated by a second aperture, 2.5 mm in diameter, placed 130 mm from the buffer gas cell. The direction of propagation of the beam is defined as the z axis (\hat{z}). This results in a molecular beam with a longitudinal velocity of $v_z \sim 120 \text{ m/s}$, with a full width at half-maximum (FWHM) spread of 40 m/s in the longitudinal velocity distribution ($T_z \sim 3.3 \text{ K}$), as determined by Doppler shift fluorescence spectroscopy. The transverse temperature of the molecular beam after the collimating aperture is $T_{\perp} \sim 25 \text{ mK}$.

Following the collimating aperture, the molecular beam travels to a 10 cm long interaction region. Cooling lasers, with a FWHM beam diameter of $\sim 3 \text{ mm}$, make 11 round-trip passes through the interaction region, yielding a molecule-laser interaction time of $t_{\text{int}} \sim 275 \mu\text{s}$. The multipass consists of a pair of mirrors and $\lambda/4$ wave plates to provide the correct polarization of light for the MOT.

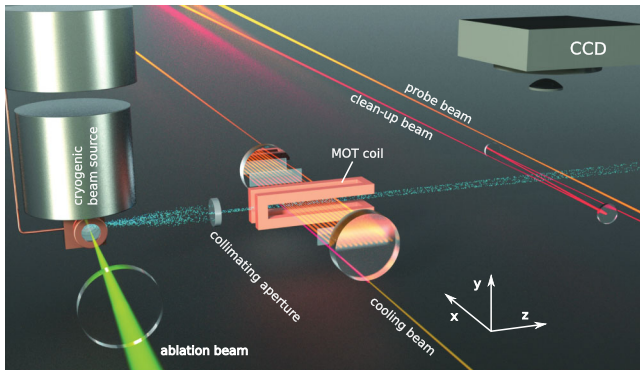


FIG. 2 (color). Depiction of the MOT apparatus, shown in its 1D implementation for clarity. The 2D system has cooling laser beams propagating along the y axis as well. The YO molecular beam (shown in granular blue) is collimated by an aperture and then passes through the 2D MOT in the interaction region, shown in the center. After ballistic expansion, the YO molecules are optically pumped into the vibrational ground state (clean-up beam), and the molecular beam is imaged using resonant fluorescence and a CCD camera, shown at the right.

The propagation direction of the cooling lasers defines the x axis (\hat{x}). The magnetic field coil used for the MOT has a rectangular baseball coil geometry, with dimensions of $5 \times 5 \times 15 \text{ cm}$. The coil consists of 25 turns of Litz wire in series with a tuning capacitor, forming an LC resonator with resonant frequency $\omega_0 = 2\pi \times 2 \text{ MHz}$ and quality factor $Q = 77$. Power is coupled into the MOT coils via a transformer designed to impedance match the MOT coil to a 50Ω transmission line. Assuming perfect coupling, a drive power of 20 W yields field gradients of $A_{\text{rms}} = 6 \text{ G/cm}$. We monitor the phase of the MOT field with a pickup coil and phase lock the MOT field to the polarization modulation signal [27].

Following the interaction region, the molecules traverse a 30 cm long region for ballistic expansion. Finally, the molecules enter a probe region, where they are optically pumped into the ground vibrational state with a multipass “clean-up” beam consisting of $v'' = 1, 2$ repump lasers. A retroreflected probe beam, derived from the same laser beam used for the cooling transition, propagates along \hat{x} and interrogates the molecules. Cycling fluorescence from the probe beam is collected along the y axis (\hat{y}) and imaged onto a CCD camera. To extract the transverse temperature of the molecular beam, $T_x = \sigma_{v_x}^2 m/k_B$, where $\sigma_{v_x}^2$ is the variance in the velocity distribution, $m = 105 \text{ amu}$ is the mass of YO, and k_B is the Boltzmann constant, we fit the molecular beam profile along \hat{x} to an expected functional form calculated from a Monte Carlo (MC) simulation. The spatial width of the molecular beam is dominated by the transverse velocity distribution. The MC simulation calculates the position and velocity of the molecules at the location of the probe beam using the observed molecular beam properties and calculated magneto-optical force F_{MO} [27].

Figure 3(a) shows a typical molecular beam profile after passing through the 1D MOT. Curve (i) shows the unperturbed molecular beam with initial transverse temperature

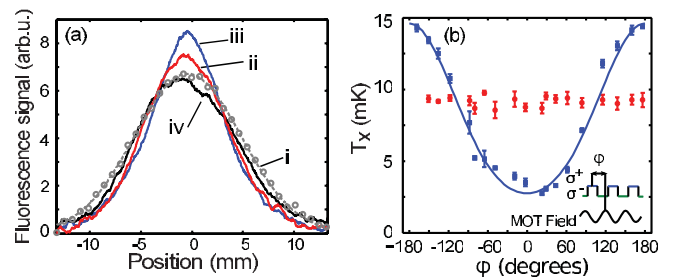


FIG. 3 (color). 1D MOT and Doppler cooling. (a) Molecular beam profiles for (i) an unperturbed beam, shown with open gray circles, and the dashed gray line as a fit, (ii) a Doppler cooled beam, and (iii) and (iv) a 1D MOT with $\varphi = 0^\circ, 180^\circ$, respectively. (b) Transverse temperature vs MOT phase φ for Doppler cooled (red, around 10 mK) and 1D MOT (blue, sinusoidal 3–15 mK), demonstrating clearly the MOT and anti-MOT phases. The solid line is a simulation using a MLRE model for the MOT force.

$T_i \sim 25$ mK, (ii) shows a Doppler cooled molecular beam (magnetic field off, $A_{\text{rms}} = 0$), and (iii) and (iv) show the molecular beam after passing through the 1D MOT with $A_{\text{rms}} \sim 6$ G/cm for the relative MOT phase $\varphi = 0^\circ, 180^\circ$, respectively. The cooling lasers are detuned by $\delta/2\pi = -5$ MHz, where $\delta = \omega_{\text{laser}} - \omega_{\text{YO}}$ is a uniform detuning of all $\nu'' = 0$ cooling lasers from their respective transitions, with $\delta = 0$ corresponding to no observable change in temperature [27]. The $\nu'' = 1, 2$ repump lasers remain on resonance. Cooling of the molecular beam is observed as a narrowing of the molecular beam profile and an increase in the number of molecules at the center. Typically, we observe that 85% of the molecules remain after cooling, consistent with the branching loss to the $A^2\Delta_{3/2}$ at a level of $\eta < 4 \times 10^{-4}$ [27,28]. Besides cooling, curve (iii) of Fig. 3(a) clearly shows the enhancement of molecules at the center of the beam due to the MOT spring force. By simply changing the phase to $\varphi = 180^\circ$, we observe an anti-MOT, where both temperature and peak molecule number deteriorate. Figure 3(b) shows the full dependence of the final temperature on φ . MC simulations, shown as a solid line, agree well with the observed phase dependence.

We observe the final cooled beam temperatures are as low as 2 mK, achieving more than a factor of 10 in cooling, yet still above the Doppler limit of 116 μK . The simulations of the Doppler cooling force indicate this is due to a finite interaction time and cooling rate [27]. The final temperature of the beam can be expressed as $T_f = T_i \times \exp[-t_{\text{int}}\Gamma_D]$, where the Doppler cooling rate $\Gamma_D = (2\beta/m)$. This implies an experimental value of $\Gamma_D \sim 5 \times 10^3 \text{ s}^{-1}$, in good agreement with the cooling rate $\Gamma_D = 8 \times 10^3 \text{ s}^{-1}$ predicted by the MLRE model. Analysis of the MOT data in Fig. 3(b) using the MC simulation yields a value of the MOT oscillation frequency of $\omega_{\text{MOT}} = \sqrt{\kappa/m} \sim 2\pi \times 155$ Hz. This agrees well with the predicted value of $\omega_{\text{MOT}} \sim 2\pi \times 160$ Hz, derived from the measured value of β and calculated magnetic field gradient $A_{\text{rms}} = 6$ G/cm. Even though the molecules traverse the MOT in a fraction of a trap oscillation, the molecular beam intensity enhancement due to the MOT is clear and can be well explained by the optical pumping rate model. This analysis quantifies both the viscous cooling and spatially dependent restoring forces, demonstrating the necessary physical components for a MOT.

While the 1D MOT provides a simple pedagogical understanding, to enhance the brightness of the molecular beam we implement the MOT in 2D. Cooling lasers then propagate along both \hat{x} and \hat{y} . Figure 4(a) shows a comparison of molecular beam profiles for the 1D and 2D MOTs. The 2D MOT exhibits an increased molecular flux and decreased cooling rate along \hat{x} , compared to the 1D MOT. The explanation for this is straightforward. Since the probe laser beam diameter is smaller than the unperturbed molecular beam diameter, the action of the MOT

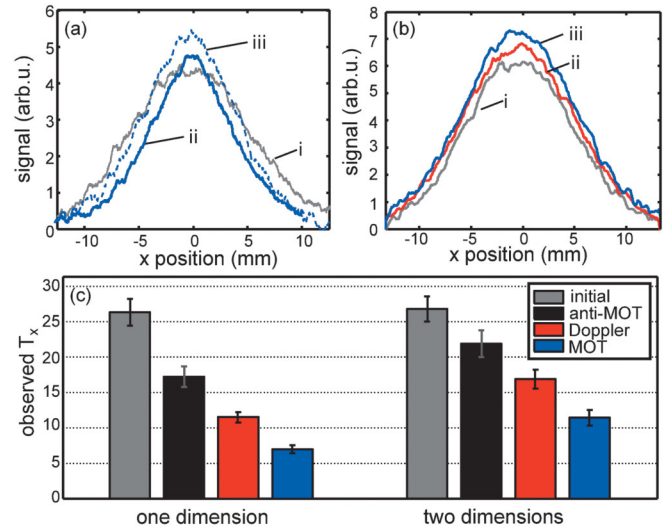


FIG. 4 (color). Comparison of 1D and 2D MOTs. (a) Molecular beam profiles for (i) an unperturbed beam, (ii) a 1D MOT, and (iii) a 2D MOT. (b) Beam profiles observed along \hat{x} with cooling along \hat{y} for (i) unperturbed, (ii) Doppler cooled, and (iii) 1D MOT. (c) Summary of observed temperatures T_x for Doppler and MOT cooling in one and two dimensions.

along \hat{y} results in an increase of detected molecules. This has been verified directly by operating the MOT along \hat{y} only and probing along \hat{x} , as shown in Fig. 4(b). The observed value of β_x in 2D is roughly half that observed in 1D. This is consistent since half the photons are now scattered along \hat{y} and do not provide any cooling along \hat{x} . Figure 4(c) compares the final transverse temperatures for Doppler cooling and the MOT in both 1D and 2D configurations. Operation of the MOT in 2D also demonstrates that there will be no unforeseen complications for a 3D MOT due to the polarizations of multiple orthogonal laser beams.

We have demonstrated a transverse MOT for polar molecules and characterize both the viscous damping force and spatially dependent restoring force. These forces lead to a factor of 10 in cooling of the transverse temperature of YO, limited only by interaction time. Extending the technique to a 3D MOT will actually solve the problem of limited interaction time, and we estimate that a 3D MOT will have a capture velocity of about 10 m/s. Loading of a 3D MOT can be achieved from a slow molecular beam [24,37]. MOT lifetimes will be limited by optical pumping into dark states [27], but this problem can be overcome by using additional repump lasers or by using a vibrational dark spontaneous-force optical trap MOT [38]. Thus, a clear path exists to a 3D MOT that produces cold, dense samples of diatomic molecules.

We acknowledge funding support for this work from AFOSR and ARO (MURI), DOE, NIST, and NSF. M. T. H. acknowledges support from the NRC. We thank K. Cossel and F. Adler for technical help.

*matthew.hummon@jila.colorado.edu

†Present address: Joint Quantum Institute, National Institute of Standards and Technology, Department of Physics, University of Maryland, Gaithersburg, Maryland 20899, USA.

‡Permanent address: State Key Laboratory of Precision Spectroscopy, Department of Physics, East China Normal University, Shanghai 200062, China.

- [1] E. L. Raab, M. Prentiss, A. Cable, S. Chu, and D. E. Pritchard, *Phys. Rev. Lett.* **59**, 2631 (1987).
- [2] J. Guest, N. Scielzo, I. Ahmad, K. Bailey, J. Greene, R. Holt, Z.-T. Lu, T. O'Connor, and D. Potterveld, *Phys. Rev. Lett.* **98**, 093001 (2007).
- [3] I. Bloch, J. Dalibard, and W. Zwerger, *Rev. Mod. Phys.* **80**, 885 (2008).
- [4] M. Saffman, T. G. Walker, and K. Mølmer, *Rev. Mod. Phys.* **82**, 2313 (2010).
- [5] M. D. Swallows, M. Bishof, Y. Lin, S. Blatt, M. J. Martin, A. M. Rey, and J. Ye, *Science* **331**, 1043 (2011).
- [6] L. D. Carr, D. DeMille, R. V. Krems, and J. Ye, *New J. Phys.* **11**, 055049 (2009).
- [7] L. R. Hunter, S. K. Peck, A. S. Greenspon, S. S. Alam, and D. DeMille, *Phys. Rev. A* **85**, 012511 (2012).
- [8] X. Zhuang *et al.*, *Phys. Chem. Chem. Phys.* **13**, 19013 (2011).
- [9] T. A. Isaev, S. Hoekstra, and R. Berger, *Phys. Rev. A* **82**, 052521 (2010).
- [10] I. C. Lane, *Phys. Chem. Chem. Phys.* **14**, 15078 (2012).
- [11] N. Wells and I. C. Lane, *Phys. Chem. Chem. Phys.* **13**, 19036 (2011).
- [12] M. Zeppenfeld, B. G. U. Englert, R. Glöckner, A. Prehn, M. Mielenz, C. Sommer, L. D. van Buuren, M. Motsch, and G. Rempe, *Nature (London)* **491**, 570 (2012).
- [13] K.-K. Ni, S. Ospelkaus, M. H. G. de Miranda, A. Pe'er, B. Neyenhuis, J. J. Zirbel, S. Kotochigova, P. S. Julienne, D. S. Jin, and J. Ye, *Science* **322**, 231 (2008).
- [14] J. D. Weinstein, R. de Carvalho, T. Guillet, B. Friedrich, and J. M. Doyle, *Nature (London)* **395**, 148 (1998).
- [15] S. van de Meerakker, N. Vanhaecke, and G. Meijer, *Annu. Rev. Phys. Chem.* **57**, 159 (2006).
- [16] E. Narevicius, A. Libson, C. G. Parthey, I. Chavez, J. Narevicius, U. Even, and M. G. Raizen, *Phys. Rev. Lett.* **100**, 093003 (2008).
- [17] S. D. Hogan, A. W. Wiederkehr, H. Schmutz, and F. Merkt, *Phys. Rev. Lett.* **101**, 143001 (2008).
- [18] B. K. Stuhl, M. T. Hummon, M. Yeo, G. Quémener, J. L. Bohn, and J. Ye, *Nature (London)* **492**, 396 (2012).
- [19] M. Di Rosa, *Eur. Phys. J. D* **31**, 395 (2004).
- [20] B. K. Stuhl, B. C. Sawyer, D. Wang, and J. Ye, *Phys. Rev. Lett.* **101**, 243002 (2008).
- [21] E. S. Shuman, J. F. Barry, and D. DeMille, *Nature (London)* **467**, 820 (2010).
- [22] J. Schoser, A. Batär, R. Löw, V. Schweikhard, A. Grabowski, Yu. Ovchinnikov, and T. Pfau, *Phys. Rev. A* **66**, 023410 (2002).
- [23] N. Wells and I. C. Lane, *Phys. Chem. Chem. Phys.* **13**, 19018 (2011).
- [24] J. F. Barry, E. S. Shuman, E. B. Norrgard, and D. DeMille, *Phys. Rev. Lett.* **108**, 103002 (2012).
- [25] K. Liu and J. M. Parson, *J. Chem. Phys.* **67**, 1814 (1977).
- [26] A. Bernard and R. Gravina, *Astrophys. J. Suppl. Ser.* **52**, 443 (1983).
- [27] See Supplemental Material at <http://link.aps.org/supplemental/10.1103/PhysRevLett.110.143001> for additional information.
- [28] S. R. Langhoff and C. W. Bauschlicher, *J. Chem. Phys.* **89**, 2160 (1988).
- [29] E. S. Shuman, J. F. Barry, D. R. Glenn, and D. DeMille, *Phys. Rev. Lett.* **103**, 223001 (2009).
- [30] J. M. Brown and A. Carrington, *Rotational Spectroscopy of Diatomic Molecules* (Cambridge University Press, Cambridge, England, 2003).
- [31] D. J. Berkeland and M. G. Boshier, *Phys. Rev. A* **65**, 033413 (2002).
- [32] W. J. Childs, O. Poulsen, and T. C. Steimle, *J. Chem. Phys.* **88**, 598 (1988).
- [33] M. Harvey and A. J. Murray, *Phys. Rev. Lett.* **101**, 173201 (2008).
- [34] B. Kloter, C. Weber, D. Haubrich, D. Meschede, and H. Metcalf, *Phys. Rev. A* **77**, 033402 (2008).
- [35] H. J. Metcalf and P. Van der Straten, *Laser Cooling and Trapping* (Springer, New York, 1999).
- [36] S. E. Maxwell, N. Brahm, R. deCarvalho, D. R. Glenn, J. S. Helton, S. V. Nguyen, D. Patterson, J. Petricka, D. DeMille, and J. M. Doyle, *Phys. Rev. Lett.* **95**, 173201 (2005).
- [37] H.-I. Lu, J. Rasmussen, M. J. Wright, D. Patterson, and J. M. Doyle, *Phys. Chem. Chem. Phys.* **13**, 18986 (2011).
- [38] W. Ketterle, K. B. Davis, M. A. Joffe, A. Martin, and D. E. Pritchard, *Phys. Rev. Lett.* **70**, 2253 (1993).